16èmes Journées de l'Hydrodynamique
27-29 novembre 2018 - Marseille

Analysis of Composite Layup Impact on Hydrodynamic Performances of Sail Yacht Flexible Hydrofoils

Analyse de l'Influence du Drapage Composite sur la Réponse Hydrodynamique d'une Structure Flexible Appliquée à un HydroFoil

V. TEMTCHING[1,2], B. AUGIER[3], T. DALMAS[1,3], O. FAGHERAZZI[4] N. DUMERGUE[3]

vanilla@seair.fr, benoit.augier@ifremer.fr, Thomas.Dalmas@ifremer.fr, fagheraz@univ-ubs.fr Nicolas.Dumergue@ifremer.fr

[1]Ecole Navale, 29240 Brest Armées [2]SEAIR, Foil Resource Center, Lorient
[3]IFREMER, Laboratoire du comportement de structures en Mer, Brest [4]ComposiTIC-IRDL, Lorient

Abstract

Composite materials are good candidates for hydrofoil manufacturing, ensuring a good balance between strength and weight. This study investigates experimentally and numerically the influence of the laminate layup on the hydrodynamic performances of a foil piercing the free surface. Four real scale hydrofoils with a constant chord, geometrically identical with different composite lay-up made up in glass or carbon fiber, are used for experiments. Mechanical properties of the foils are experimentally obtained and comparisons to numerical approaches calculating composite properties show a good consistency in the different experimental tests and good agreements of numeric and experiments (relative difference $< 10\%$) when looking at the bending stiffness. Hydrodynamic experiments are carried out in a flume for several incidences and flow stream velocities. For the same configuration, hydrodynamic performances are different from one structure to another, highlighting the impact of the composite structure. Comparisons to the numerical FSI tool FS6R is realized and shows good agreements with experiments on the orthotopic structures. This tool improves the knowledge of the FSI on composite hydrofoils which helps to improve their design and therefore the sailing yacht performances.

Résumé

Les matériaux composites représentent un excellent compromis alliant propriétés mécaniques élevées et masse réduite pour la fabrication d'un hydrofoil performant. Cette étude analyse expérimentalement et numériquement l'impact du drapage composite sur la réponse hydrodynamique des hydrofoils. Quatre foils d'échelle réelle, de même géométrie mais de drapages différents sont fabriqués en fibres de verre et carbone. Des comparaisons entre les résultats expérimentaux de caractérisation mécanique des foils et des outils numériques calculant les propriétés des matériaux composites montrent une bonne cohérence entre les différentes méthodes expérimentales utilisées et une concordance avec les approches numériques présentatnt des écarts relatifs inférieurs à 10% sur la rigidité en flexion des hydrofoils.
Des expériences hydrodynamiques son réalisées dans un bassin de courant pour 2 nombres de Reynolds et plusieurs incidences. Les comparaisons des differents hydrofoils entre eux montrent dans les mêmes configurations, des performances hydrodynamiques impactées par le drapage des strutures. Une comparaison des déplacements et efforts expérimentaux avec les résultats issus de l'outil numérique "FS6R" développé pour des calculs d'interaction fluide structure montre de bon résultats sur ces structures orthotropes (écarts relatifs $< 10\%$).

Nomenclature

FSI: Fluid structure Interactions
POM: Polyoxymethylene material
VAM: Variational Asymptotic Method
FFT: Fast Fourier Transform
VLM: Vortex Lattice Method
LT: Laminate Theory
V: Velocity [m/s]
UD: Unidirectional ply
V_f[%]: Volume fiber
V[m/s]: fluid velocity
FSI: Fluid Structure Interactions

I – Introduction

For the top high performances foiling yacht design, bend-twist coupling can be a good approach to control the lifting force through Fluid Structure Interactions with a passive adaptive approaches. Recently, works on bend-twist coupling in composites show that the phenomenon depends on layout properties and can be observed with plies orientations.
Figure1 shows the evolution of α[%], the limit of bend-twit coupling with the fibers orientation for glass and carbon fiber and the maximum coupling is obtained with $\pm 25°$.

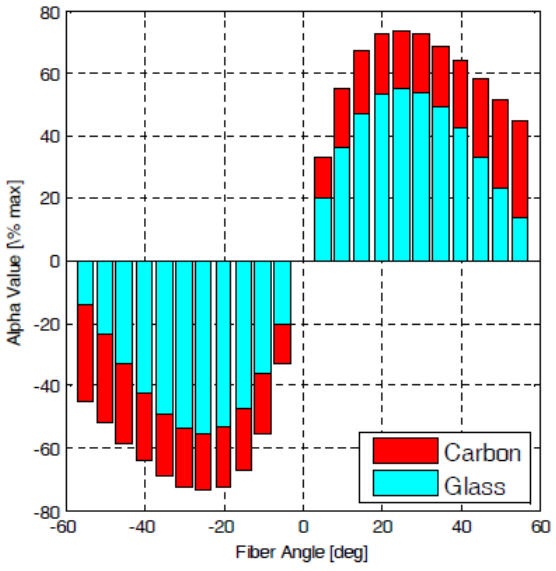

$$\begin{bmatrix} EI & -g \\ -g & GJ \end{bmatrix} \begin{bmatrix} b \\ t \end{bmatrix} = \begin{bmatrix} M_b \\ M_t \end{bmatrix} \qquad \alpha = \frac{g}{\sqrt{EI \cdot GJ}} \qquad -1 \le \alpha \le 1$$

Figure 1: Limit of bend twist coupling with the plies orientation. [1]

Indeed, Bend twist coupling is a target effect for highly loaded structures to reduce the loads by reducing the incidence at the tip. [3] shows that this behavior decreases the load and modifies the tip vortices. [5], [7] investigated the effect of this coupling on natural frequencies and mode shape to improve the design and the control of composite structures.[4] investigated the effect of bend-twist coupling on the loads in wind turbines with super element blade definition. They discover that with an appropriate composite layup, this coupling leads to loads alleviation and drastically reduces the damage in the structures.
The present study investigates the impact of composite layup on hydrodynamic performances of an hydrofoil piercing the free surface in the case of large displacements up to 10% at the tip. Four composite hydrofoils made up of carbon or glass fibers are used for the experiments.
The second chapter of this paper presents the manufacturing of the foils and the mechanical characterization of both hydrofoils and specimens by bending tests, vibration analyses and tensile tests.
To assess the uncertainty of theoretical models developed for composite properties calculations, a comparison of those results to three numerical approaches is perormed: the first approach is developed at IFREMER and stands on the laminate theory (LT), the second one "FS6R", developed in this project stands on a Variational Asymptotic Method (VAM) applied to a non linear composite beam theory [6] while the third one is the commercial software ABAQUS, using its Meshed beam cross-sections function which allows the description of a beam cross-section including multiple materials and complex geometry.
The third chapter depicts hydrodynamic experiments carried out in a flume for several incidences and flow stream velocities, with FSI and ventilation effects. The foils displacements and hydrodynamic loads are measured and compared to a reference case corresponding to a rigid body computation. Vibration analysis are also performed to quantify the resonance frequencies in water. In this part we also focus on the validation of the tool "FS6R", a coupled approach between the potential flow code AVL, and an internal code based on beam the-

ory by finite elements that integrates cross section properties calculation. "FS6R" aims to compute FSI on a hydrofoil during the predesign process. [8] presents the description of this tool and its validation on an isotropic material giving results in a very good agreement with experiments.
The principal objective of this paper is first to find out if bend-twist coupling modifies the hydrodynamic performances of the composite hydrofoils through FSI in the configurations and for the structures investigated; and second to validate "FS6R" on composite materials.

II – Hydrofoils characterisation

This chapter describes the manufacturing and the characterization tests of the hydrofoils in air.

II – 1 Hydrofoils Manufacturing

Four hydrofoils are manufactured by SEAIR, the industrial partner of this research work. The manufactured foils are structures of $1.35m$ span and $0.114m$ constant chord. The section is a NACA 0015 sandwich structure made of an AIREX web and laminated skin. The different layups and associated materials are given in Table 1 and Figure 2 shows the general structure of the foils in a CAD model and the manufactured section. In the section, the green AIREX is clearly visible, the black part is the glue *Spabond*345 and the white part is the glass fiber.

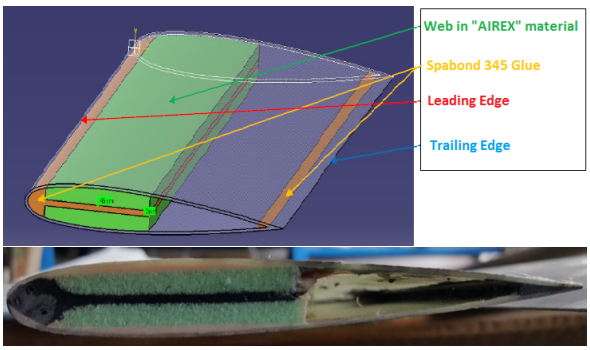

Figure 2: Hydrofoil composition and P_2 manufactured section.

The manufacturing of the foils is realized by a vacuum lamination method and the overall process goes through several steps including : stratification in the mold, bounding of the web, intrados-extrados glueing, demolding, foil base manufacturing and finishing.
The foils base are directly manufactured on the foils by molding using a 3D printed piece to position the hydrofoil in the mold as shown in Figure 3.

Foils	Material	layup
P_1	Epoxy-Glass	$[\pm 45)_2/0_{0.5}]_{sym}$
P_2	Epoxy-Glass	$[(90/-45/0_{0.5}]_{sym}$
P_3	Epoxy-Glass	$[(90/45/0_{0.5}]_{sym}$
P_4	Epoxy-Carbon	$[(90/0)_{sym}]$

Table 1: Layup definition and materials.

Parallel to this, four plates of 200×200 mm^2 with the layup of Table 1 are also manufactured for the tensile specimens.

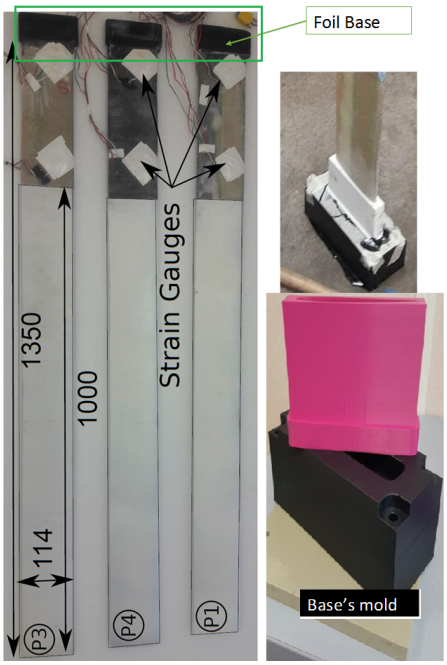

Figure 3: Finished hydrofoil with stain gauges location showing the foil base in black. Along side is the black mold and the pink 3D printed piece.

II – 2 Mechanical characterization

First this part describes the experiments realized to determine the bending stiffness of the hydrofoils. The laminate theory is briefly describes in the second part and results are presented in the third section through a comparison with the numerical approaches.

II – 2.1 Experimental setup

The rigid test bench shown in Figure 4 is realized for the purpose of these experiments. The foil is bolted to the bench through the foil base in cantilevered-free boundary conditions and the clamping conditions for these tests are identical for the hydrodynamic experiments. A vertical load is applied through calibrated masses and the vertical displacements of the structures are recorded thanks to a laser rangefinder.
The same system is used for bending and vibration analyses when a conventional tensile setup is used for the tensile experiments on the laminate specimens (Figure 5).

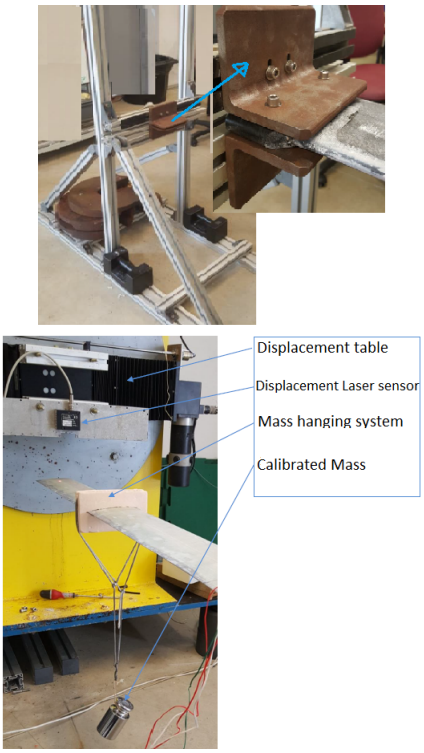

Figure 4: Bending and vibration experimental setup.

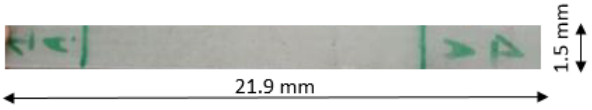

Figure 5: laminate specimen in layup P_1 used for tennsile test characterization.

II – 2.2 Tests

Four masses: $M_1 = 518g$, $M_2 = 1018g$, $M_3 = 2018g$ and $M_4 = 3018g$ are used to applied the load during the tests.

Bending Tests
Figure 6 shows the bending test of a foil with M_3 load. For all the configurations the load $F = M \times g$ is applied at the distance supposed to be the application point of the hydrodynamic resultant loads, $L = 850\ mm$ from the root. The laser measures the vertical displacement Y of the foil at the tip, located at distance X from the root and the bending stiffness EI of the structure is calculated by (1).

$$EI = \frac{FL^2(3X - L)}{6Y} \tag{1}$$

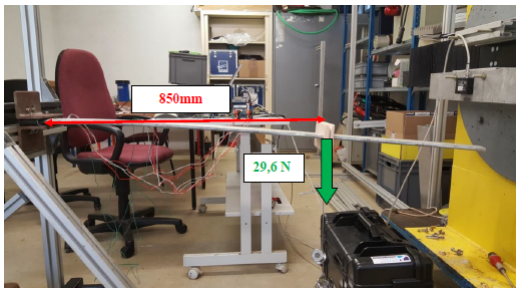

Figure 6: Bending Test M_2

Vibration Analyses
The structure is manually excited and the laser measures the vertical displacement over time at the tip. Vibration test and bending test are carried out together.Several tests are performed and averaged in the results . The bending stiffness EI of the structure from vibration analysis is then calculated by (2).

$$EI = \left(\frac{2\pi f_i L^2}{\lambda_i^2}\right) m \tag{2}$$

f_i: the natural frequency of the mode i
λ_i: a number associated to the proper mode i, depending of the boundary conditions
m:the structural weight per unit of length
L: the length of the structure.

The natural frequency is obtained by a FFT on the temporal signal recorded by the laser. Figure 7 shows the vibration response of the layup P_1 in the first vibration test.
The FFT of the signal clearly shows a well defined peak corresponding to the natural frequency of the foil in its first bending mode of $3.9Hz$ giving a bending a stiffness of $EI = 157.87N.m^2$.

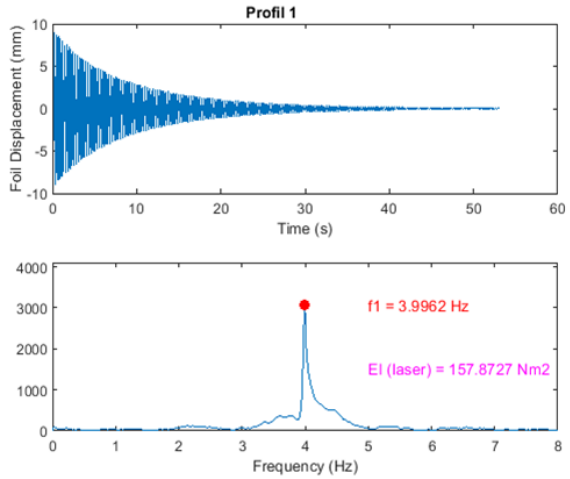

Figure 7: Vibration response of P1, test vib_1.

Tensile Tests

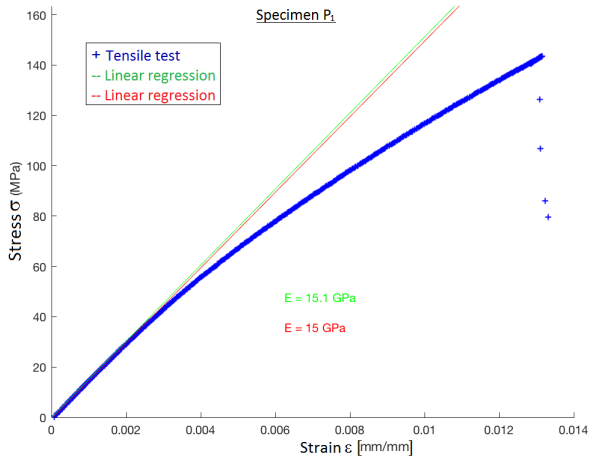

Figure 8: Stress vs strain for tensile test on the specimen layup P_1.

Tensile tests are carried out on specimens of the different layup whose dimensions comply with the ISO 527 standard. A specimen is fixed in the jaws of the machine (Figure 6) and the displacement speed are fixed. As output of the machine, the temporal evolution of the force and deformation are recorded.
The young modulus E corresponds to the slope of the curve $\sigma = f(\epsilon)$ as shown in Figure 8 for the specimen P_1 giving a young $E = 15\ Gpa$.
σ is the elastic stress and ϵ is the strain.
EI of this layup is obtained by the product of E from the tensile test to the inertial momentum I of the hydrofoil section, taking into account the skin thickness of the laminates.

II – 2.3 Laminates theory

A tool based on laminates theory to access the mechanical properties of the composites, developed at IFREMER is used.
Laminates theory describes a ply in its membrane plane and calculates its properties E_l, E_t, G_lt, ν_{lt}, e_p as a function of the fibers and resin properties E_f, E_m, G_m, ν_f, ν_m.
[2] describes the theory and shows the functions calculating the plies properties in the membrane plane and the equivalent properties of a stratified structure in all the direction.
EI is obtained by the product of E from the laminates theories by the inertial momentum I calculated with the real skin thickness.
The commercial software ABAQUS and the mechanical part of "FS6R" presented in the next chapter, are also used to calculate the equivalent EI of the structures.
Table 2 gives the UD properties used in this part. The layup P_1uses the Glass2 when layupP_2 and P_3 uses the Glass1.

Material	Carbon	Glass1	Glass2
$E_l[GPa]$	120	54	45
$E_t[GPa]$	10	10.4	10
$G_{lt}[GPa]$	4	3.9	5
ν_{lt}	0.362	0.25	0.25
$e[mm]$	0.3	0.2	0.2
$V_f[\%]]$	55	60	60

Table 2: Mechanical properties of the unidirectional plies used in the Laminate theory, the matrix is epoxy.

II – 2.4 Results

Figure 9 compares the bending stiffness EI obtained experimentally with the numerical results from the laminates theory, ABAQUS and FS6R for all the layups P_1, P_2, P_3 and P_4 (see Table 1).
The y-axis gives the EI values and the x-axis represents the different methods:
vib: the mean value of the vibration tests .
M_i: The bending test using the mass M_i as load.
LT: Laminate theory using the properties defined in Table 2.
ABQ, FS6R: ABAQUS and FS6R.
For each experiment, many tests are realized and the average results are presented.

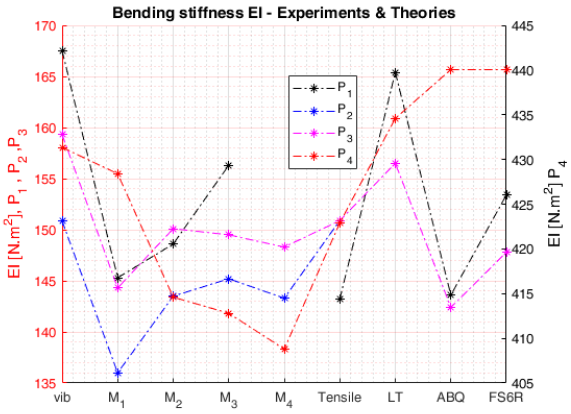

Figure 9: Comparison of Bending stiffness from numerical and experimental approaches.

Figure 10 shows the relative difference using the the average of experimental values as reference. For each foil,the bending stiffness calculated by all the methods are close with a relative difference less than 10%.

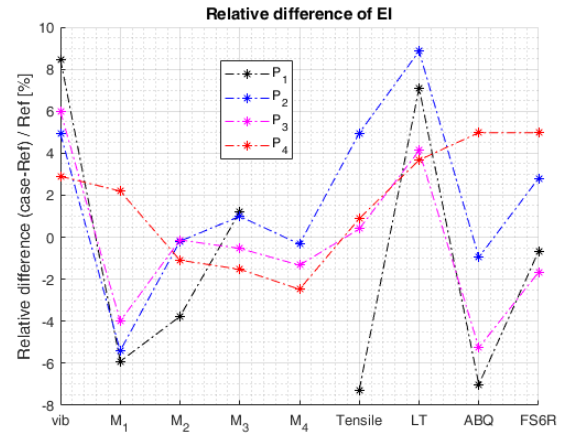

Figure 10: relative difference of EI computed with average values of experimental tests.

All the experimental tests, bending, tensile and vibration tests are close to each other with a relative difference of around less than 5% excepts P_1 with tensile and vibration which dive discrepancies up to 8%.
P_4 has the highest stiffness values due to the use of carbon fibers instead of glass.
The numerical approaches give the same results for P_2 and P_3 because the bending stiffness is not sensitive to the sign of plies orientation; for that reason only one specimen is used in the tensile test to characterize P_2 and P_3.
Laminate theory gives results with less than 10% difference when the theoretical volume fiber is used. The volume fiber can have an important effect on the characterization. Calcination tests have been carried out but the results need more post processing.
FS6R calculations give values similar to the laminate theory with differences around 5% when ABAQUS is higher but the discrepancies stay under 8%.

All these experimental methods used to characterize the bending stiffness of the foils give similar results and the numerical approaches are in good agreement with the experiments, giving relative differences less than 8%.

III – Hydrodynamic experiments

III – 1 Experimental setup

The experimental setup of hydrodynamic experiments is presented at Figure 11.
They are carried out at IFREMER Lorient in a flume of 2.5 m in the flow direction and 1.5 m height with a maximum velocity of 1 m/s.
A 6-DOF balance giving the efforts and moments is used and a telemeter laser measures the lateral displacements of the foils at 3 different heights corresponding to well located positions on the span (Figure 12). The balance follows the foil motion so its measures the efforts in the foil reference axes (X,Y,Z).

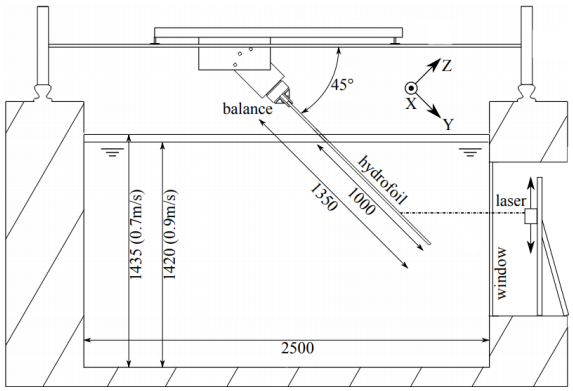

Figure 11: Hydrodynamic flume used for hydrodynamic experiments showing an hydrofoil mounted on the balance at 45° and the laser.

As depicted on the picture, the foils are piercing the free surface and mounted cantilevered-free on the 6-axis balance, oriented at 45° with the water free surface. The clamping conditions are the same used for the previous tests, the flow is aligned with X-axis.

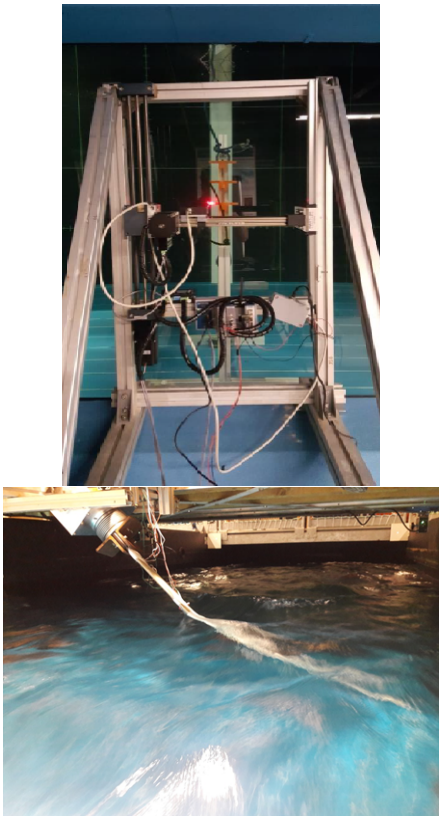

Figure 12: Hydrodynamic experiment showing the foil clamped on the balance with the strain gauges and the laser.

This tilt of 45° prevents on one hand the foil from touching the bottom of the shallow flume and avoid the ground effects. On the other hand the foil gets close to the laser and thus ensures that it stays in the laser operating domain. The foils are all equipped by 2 strain gauges installed at respectively 350 mm and 250 mm from the embedding.
Two speeds ($0.7m/s$, $0.9m/s$) and several angles of attack ranging in $[-3°, 9°]$ are investigated. The free surface height varies with the velocity: $1.435m$ for $0.7m/s$ and $1.42m$ for $0.9m/s$.
Results are described after the following section presenting FS6R computations.

III – 2 FS6R Computations

FS6R is a code dedicated to the preliminary stages of foils design to model and to analyze fluid structure interactions. It stands on the lifting line method and beam theory by finite elements.
After the definition of the foil geometry, the material and the configurations to simulate, the hydrodynamic flow is resolved by the open source tool AVL which performs a VLM inviscid 3D calculations on the whole surface and provides the 3D hydrodynamic coefficients. A viscous correction is achieved by XFOIL which performs 2D viscous calculations.
The structural analysis is performs by an in house code standing on beam theory by finite elements. [8] describes FS6R in details and presents its validation on a 3D trapezoidal foil in POM material. This code uses the Variational Asymptotic Method describes in [6] to calculate the properties of a given section associated to a material such as: the shear center, torsional center, young modulus, inertia, shearing stiffness GJ,...
At an output of FS6R calculation, we get the efforts applied on the structure and the distorted shape.

III – 3 Results

Due to inconsistencies with different measures, some configurations are dismissed.

Efforts

Figure 13 illustrates the bending moment recorded by the balance (located at the cantilevered end) between all the foils for the two velocities investigated. The results are compared to a rigid calculation computed with FS6R, only the fluid calculation is performed and the efforts are reduced to the embedding to calculate the bending moment.
For $V = 0.7\ m/s$, P_1, P_3 and P_4 appears to be very similar and slightly higher than the rigid moment when P_2 is clearly lower than the rigid moment, which is consistent with P_2 layup $[(90/-45/0_{0.5}]_{sym}$.
This behavior increases when the velocity rises and the observed trend remain the same: P_1, P_3 and P_4 values are close when P_2 is highly lower than the rigid moment and the global trend tends to be $P_2 < Rigid < P_3 < P_4 \sim P_1$. Only P_2 shows a behavior significantly different than the rigid one with a bending moment smaller than the rigid case of 20 to 40% at $V = 0.7\ m/s$ and 40 to 75% at $V = 0.9\ m/s$.

The origin of all these differences can be found in an existing twist, oscillations observed during the tests or the locally modification of

the apparent foil's profile seen by the flow, due to its structural displacements under the hydrodynamic loads. More investigations are performed in the following results through the comparison to FS6R.
The moment being a direct image of the lift force, these results shows that lift force is significantly impacted by the composite layups.

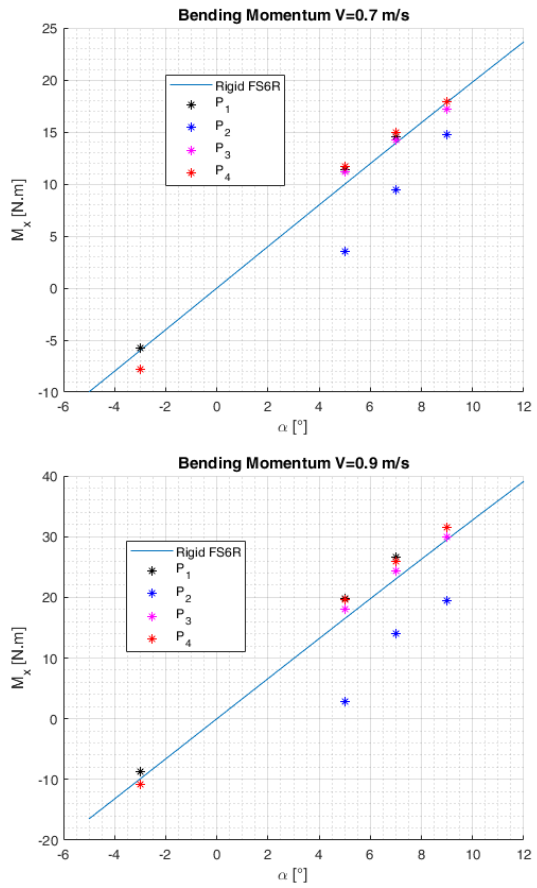

Figure 13: Experimental bending moment compared to the rigid calculation with FS6R.

FS6R VS Experiments

Figure 14 compares FS6R moments calculated with FSI loop to experiments on the bending moment.
FSI calculations made on the different foils do not differentiate the moments but only the lift direction due to the bending.
Note that, VAM method also allows the calculation of the torsional modulus GJ.
Comparison of GJ from FS6R and Abaqus shows discrepancies up to 58% with the layups when Abaqus is used as reference. No twist were found in FSI calculations for these configurations.

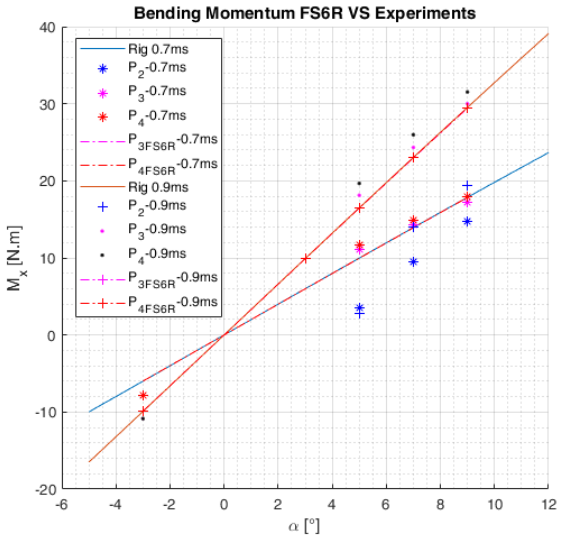

Figure 14: Experimental bending moment compared to FS6R for P_2, P_3 and P_4.

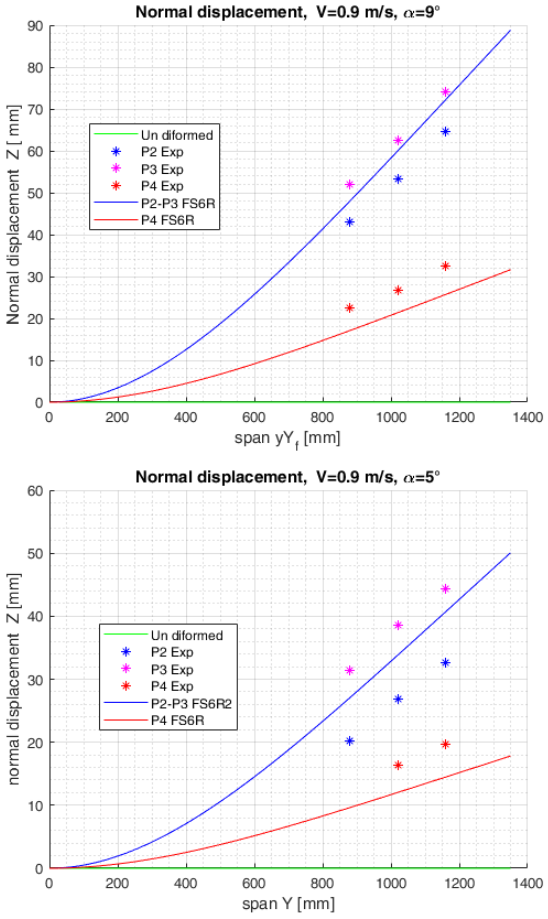

Figure 15: Displacements of the foils normal to the span, computed with FSI simulation.

Fig 15 shows the displacements normal to the span direction, computed by FS6R in a

comparison to the experimental measurement for P_2, P_3 and P_4 and for the two velocities investigated. The trend previously observed in the bending moment is well repeated in the displacements.
Work are still in progress in this part to model the bend twist coupling. To get rid of this limitation, a correction with a calculated twist is performed.

FS6R corrected: experimental bend-twist coupling
The angle of bend twist coupling is obtained by converting the difference between the experimental moment to the rigid moment into angles.
The rigid M_x moment follows a linear evolution described by (3) and (4) for the two velocities. Table 3 shows the computed angles for $V = 0.9m/s$, α is the angle of attack and, the values contained in the table are the twist angles.

$$Mx_7 = 1.98 \times \alpha - 5.8e^{-3} \quad (3)$$
$$Mx_9 = 3.28 \times \alpha - 9.5e^{-3} \quad (4)$$

$\alpha[^\circ]$	P_1	P_2	P_3	P_4
-3	0.35		-0.29	-0.28
5	1.02	-2.17	0.5	0.97
7	1.093	-1.86	0.398	0.9
9		-1.17	0.15	0.61

Table 3: Bend-twist coupling 's angle in [°] computed with experimental measurements for $V = 0.9m/s$.

For this part the mean value of experimental bending stiffness is used FS6R and the computed displacements are shown in Figure 16.
For $V = 0.9m/s$, FS6R match perfectly with experiments when $V = 0.7m/s$ displays differences in both approach especially with P_2 layup. The relative difference is presented in Figure 17.
Near the tip, the relative difference is very low (under 5%) for many cases an stays under 10%. This gap increase when we get close to the root of the foil but globally it is less than 15%.

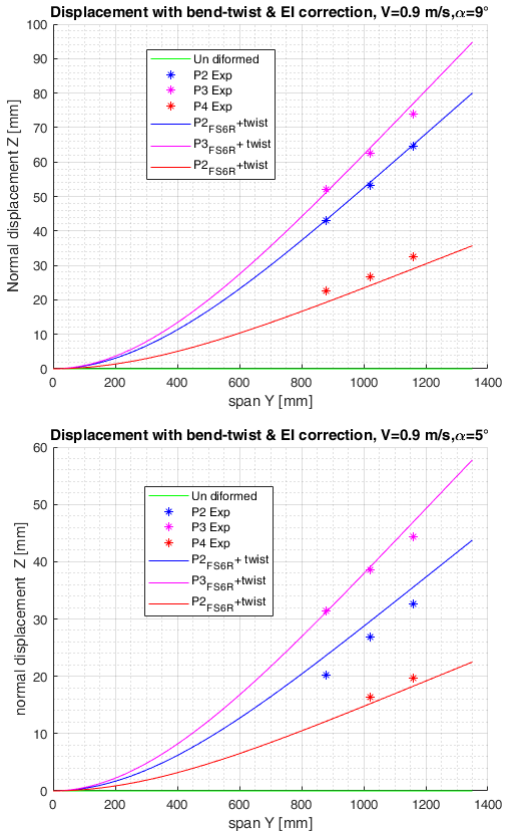

Figure 16: FS6R VS experiments: displacements for P_2, P_3 and P_4 .

Those remaining errors highlights the inaccuracy in the calculation of the twist angle and the need to determine a better approach. It also depicts that if the basic properties of the fibers and resins are well set, FS6R can compute the efforts and displacements on a composite hydrofoil under hydrodynamic loads with a relative error less than 10% in the case of no bend-twist coupling.

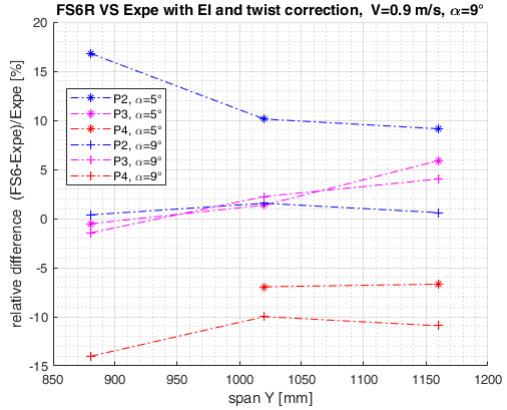

Figure 17: FS6R VS experiments: displacements for P_2, P_3 and P_4 .

III – 4 Vibration analysis

This part presents the results of the vibration analysis in water.

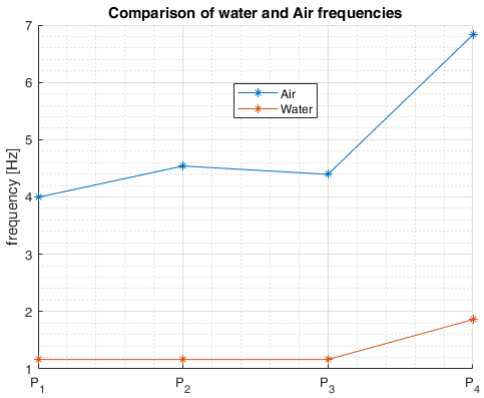

Figure 18: Hydrofoil natural frequencies in air and water.

Figure 18 shows the difference in natural frequencies in air and in water for all the hydrofoil layups. The frequency is drastically reduced in water because of the added mass.
This added mass adding a term to the foil mass is computed using (Eq. 2) and the results are presented in Table 4.

foil	P_1	P_2	P_3	P_4
A. M. $[kg/m]$	10.03	10.43	9.73	10.84

Table 4: Added masses.

The trends are the same as the frequencies and, P_2 is 7.2% higher than P_3.

IV – Conclusion

This work studied experimentally and numerically the influence of composite layup in the hydrodynamic response of an hydrofoil piercing the free surface.
A first comparison of bending stiffness between experimental methods show a consistency between them and, those results compared to numerical approaches shows good agreements (less than 10% for the relative difference).
Hydrodynamics experiments carried out in a flume for two speeds and different angles of attack show differences in the lift response (through the bending moment) with a rigid case due to the displacements of the foils.
FSI are clearly observed in these results depicting the appearance of a negative twist with the hydrofoil layup P_2 $[(90/-45/0_{0.5}]_{sym}$ and a positive twist with the other layups.
The comparison of FS6R results with experiments on the bending stiffness give low relative difference of around 5%. FS6R is able to compute bend twist coupling leading to discrepancies with experiments up to 30% on the displacements.
The coupling is replaced by a simple approach based on experimental observations. This approach together with the experimental bending stiffness EI reduces the FSI differences down to 10% on the displacements computed by FS6R. These remaining errors are more likely due to some measurement mistakes, the post-processing process and the twist calculation.
Further efforts on this project are realized to numerically detect the twist with FS6R and get a better consistency to the real behavior of the composite structures.

References

[1] M. Capellaro. Design challenges for bend twist coupled blades for wind turbines and application to standard blades. In *Proceedings of Sandia Wind Turbine Blade Workshop*, 2012.

[2] D. Gay. *Materiaux composites; 3rd ed.* Traité des nouvelles technologies. Hermès, Paris, 1991.

[3] L. M. Giovannetti, J. Banks, M. Ledri, S. Turnock, and S. Boyd. Toward the development of a hydrofoil tailored to passively reduce its lift response to fluid load. *Ocean Engineering*, 167:1–10, 2018.

[4] O. Gozcu, T. Farsadi, C. Tola, and A. Kayran. Assessment of the effect of hybrid grfp-cfrp usage in wind turbine blades on the reduction of fatigue damage equivalent loads in the wind turbine system. In *Proceedings of the 9th International Workshop on Water Waves and Floating Bodies (10.2514/6.2015-0999)*, 2015.

[5] M. O. Gözcü and A. Kayran. Investigation of the effect of bending twisting coupling on the loads in wind turbines with superele-

ment blade definition. *Journal of Physics: Conference Series*, 524(1):012040, 2014.

[6] D. H. Hodges. *Nonlinear Composite Beam Theory,* . 78-1-56347-697-6. American Institute of Aeronautics and Astronautics, 1, 2006.

[7] S. E. Rohde, P. G. Ifju, B. V. Sankar, and D. A. Jenkins. Experimental testing of bend-twist coupled composite shafts. *Experimental Mechanics*, 55(9):1613–1625, 2015.

[8] O. F. V. TEMTCHING, B. AUGIER and J.-A. A. D.R. An experimental and numerical study of fsi applied to sail yacht flexible hydrofoil with large deformations. In *Proceedings of 9th International Symposium on Fluid-Structure Interactions Flow-Sound Interactions Flow-Induced Vibration and Noise (Toronto Canada)*, 2018.